Materials Horizons

ROYAL SOCIETY OF CHEMISTRY

COMMUNICATION

View Article Online
View Journal

Cite this: DOI: 10.1039/d5mh01674f

Received 1st September 2025,
Accepted 10th October 2025

DOI: 10.1039/d5mh01674f

rsc.li/materials-horizons

Competition between mirror symmetry breaking and translation symmetry breaking in ferroelectric liquid crystals with increasing lateral substitution

Grant J. Strachan, * Ewa Górecka and Damian Pociecha

The recently discovered heliconical ferroelectric nematic (N_{TBF}) phase is a unique example of spontaneous chiral symmetry breaking in a proper ferroelectric fluid. In this study, we investigate four homologous series of mesogenic compounds, differing in the degree of fluorination of the mesogenic core and bearing lateral alkoxy substituents of varying lengths, to understand how molecular architecture influences the formation and stability of the N_{TBF} phase. Increasing the length of the lateral chain lowers the phase transition temperatures and suppresses smectic layer formation, enabling the emergence of the N_{TBF} phase which replaces the orthogonal ferroelectric smectic A (SmA_F) phase. This indicates a competition between lamellar and heliconical polar ordering, driven by the interplay of strong molecular dipoles and the self-segregation of chemically incompatible molecular segments that typically favour layered structures. Notably, the N_{TBF} phase in these compounds exhibits exceptionally short helical pitch lengths, on the order of a few hundred nanometers, as revealed by selective light reflection and atomic force microscopy (AFM). Furthermore, for one of the studied compounds AFM imaging revealed a regular array of screw dislocations within the N_{TBF} phase, suggesting a possible link to more complex modulated or twist-grain-boundary-like structures.

New concepts

Liquid crystal (LC) phases exhibiting proper ferroelectricity combine fluidity with extremely high values of spontaneous electric polarisation and have a vast array of potential applications – if their formation can be controlled. However, the relationship between molecular structure and the formation of these new polar phases are still poorly understood. Within this new class of polar soft matter, the formation of spontaneously chiral structures is an intriguing but rare phenomenon, which is highlighted by the highly unusual properties of the heliconical ferroelectric nematic (N_{TBF}) phase. We have discovered that designing molecules with structural features which disrupt the formation of layered (smectic) phases can reveal the N_{TBF} phase. This suggests that there is a competition between the interactions driving layer formation and those promoting heliconical structure. This new insight enabled us to prepare a selection of mesogens forming the N_{TBF} phase. AFM studies of one material revealed an unexpected morphology, featuring a regular array of screw dislocations which may hint at the possibility of even more structurally complex phases within this family of polar liquid crystals.

Introduction

The emergence of chiral structures from achiral building blocks is an intriguing phenomenon that has caught the interest of those working in both fundamental research and in the development of new technologies. A newly discovered liquid crystal phase, the heliconical ferroelectric nematic phase (N_{TBF}), is a prime example of this.[1] The N_{TBF} phase is a member of the recently discovered, and rapidly growing, family of proper ferroelectric liquid crystals, which began with the 2017 discovery of the ferroelectric nematic (N_F) phase,[2–4] and now includes orthogonal SmA_F, tilted SmC_F, and heliconical SmC_P^H layered phases as well as phases with antiferroelectric order N_X/SmZ_A/M_{AF}/N_S and SmA_{AF}.[1,5,6] (Sketches of these phases are given in Fig. 1). In the N_{TBF} phase, the director follows a heliconical trajectory, being tilted with respect to the helical axis, and the helical pitch is typically reported to be on the micron scale, comparable to the wavelength of visible light. As the breaking of mirror symmetry occurs spontaneously, both left- and right-handed helices are formed (Fig. 1).

In these recently discovered longitudinally polar phases, ferroelectricity arises directly from the interactions of molecular dipoles. This differs from previously known ferroelectric LCs in which ferroelectricity occurs as a secondary effect, for example induced by molecular chirality or the close packing of bent-core molecules. These new proper ferroelectric phases, despite their fluid nature, exhibit very high spontaneous polarisation reaching values comparable to solid, crystalline ferroelectrics. There has been a great deal of attention devoted to these new phases, focusing both on their fundamental properties as well as their potential applications. These systems offer

Faculty of Chemistry, University of Warsaw, ul. Pasteura 1, 02-093 Warsaw, Poland. E-mail: g.strachan@chem.uw.edu.pl

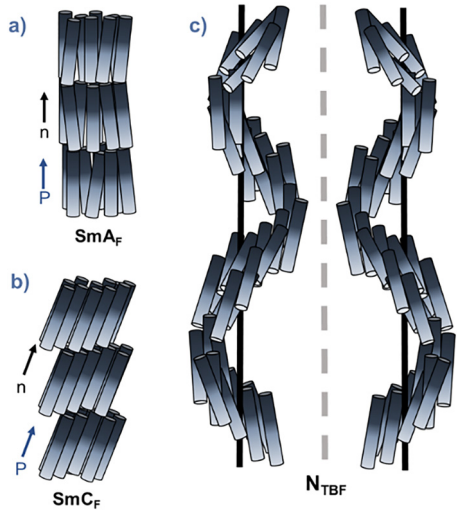

Fig. 1 Sketches of the ferroelectric smectic A (SmA_F) phase (a); the ferroelectric smectic C (SmC_F) phase (b); and the heliconical ferroelectric nematic (N_{TBF}) phase (c) with helices of opposite handedness shown. Black arrows represent the orientation of the director (*n*) and blue arrows the polarisation direction (*P*).

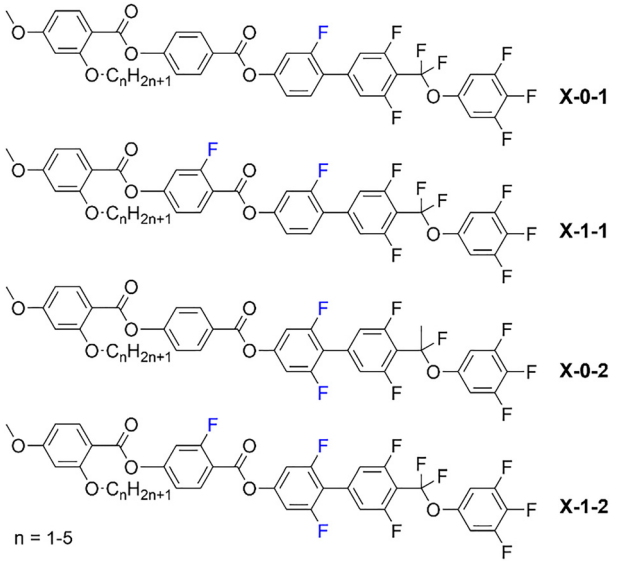

Fig. 2 The general molecular structure of the 4 homologous series reported here.

unique insight into the interplay between electrostatic and elastic forces in soft materials. While the properties of paraelectric liquid crystal phases are often considered in terms of elastic energies and deformations, the proper ferroelectric mesophases bring the role of electrostatic interactions to the fore. This has led to several interesting discoveries, including the apparent 'tendency to twist' found for highly polar molecules within fluid phases. While chiral states have been reported in both the N_F[7] and SmA_F[8] phases, the clearest example of this is still the N_{TBF} phase. The chiral symmetry breaking observed in the N_{TBF} phase is believed to be driven by interactions between the strong electric dipoles of the molecules, which promote a non-colinear arrangement and lead to the formation of heliconical structure.[1] This has been compared to the Dzyaloshinskii–Moriya interaction observed in magnetic systems.[9]

However, the N_{TBF} phase is still extremely rare, with only a few examples reported to date, and the precise molecular features required for its formation are not understood. To study this unusual new phase, and to develop its application potential, it is vital to understand the influence of molecular architecture on the formation of the phase, and to expand the range of molecules showing this phase.

Our previous studies[10] showed that an uneven variation in the electron density along the long molecular axis would promote the formation of the polar smectic phases (SmA_F and SmC_F) due to the self-segregation effect of chemically non-compatible units; while a more uniform distribution of electron density favours the N_F phase. For a material, which is intermediate between these two extremes we observed the N_{TBF} phase. This is somewhat similar to trends seen for two homologous series of polar liquid crystals, both with a terminal alkyl chain, reported by Karcz *et al.*,[1] and by Nishikawa *et al.*[11] In both cases, the N_{TBF} phase (referred to as the $^{HC}N_F$ phase in ref. 11) was observed at an intermediate chain length, with shorter homologues only forming the ferroelectric nematic phase, while at longer chain lengths, the N_{TBF} phase was replaced by smectic behaviour.

Considering these observations, we hypothesised that mesogens with molecular features expected to suppress smectic ordering may promote the formation of the N_{TBF} phase. To test this, we have selected four structures (Fig. 2) forming either SmA_F or N_{TBF} phases and increased the length of their lateral alkoxy substituents. This structural change decreases the length-to-breadth ratio of the molecules and disrupts side-to-side interactions between neighbouring molecules, and both effects are expected to decrease the tendency for layer formation. Each compound is given a code, **X–Y–Z**, where **X** represents the length of the lateral alkoxy chain: **M** (methoxy) OCH_3, **E** (ethoxy) OC_2H_5, **P** (propyloxy) OC_3H_7, **B** (butyloxy) OC_4H_9, **Q** (pentyloxy) OC_5H_{11}. **Y** and **Z** are the number of fluorine substituents on the second and third aromatic rings, respectively.

Methods

The full description of synthetic methods and structural characterisation of the reported compounds, and experimental details are given in the accompanying SI.

Synthesis

The synthesis of the reported materials followed the approach outlined in Scheme 1. Starting from methyl 3-hydroxy-4-methoxybenzoate, a Williamson ether reaction was used to attach the appropriate lateral chain using the corresponding alkyl bromide or iodide. The methyl ester was deprotected under basic conditions, and the resultant acids underwent

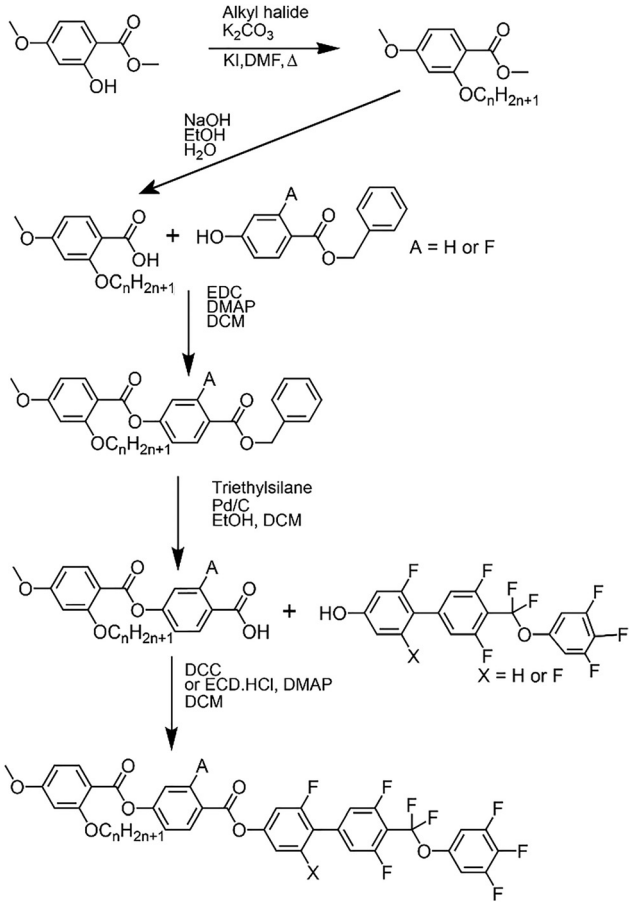

Scheme 1 The general procedure for synthesis of studied compounds.

EDC mediated esterification with the required benzyl protected phenols. The resultant esters were deprotected *via* palladium catalysed hydrogenation. The acids thus obtained underwent a final esterification using either EDC·HCl or DCC as the coupling agent, to yield the target compounds.

Assignment of liquid crystal phases

Preliminary phase assignments were carried out using polarised-light optical microscopy, and phases were identified based on the observation of characteristic optical textures (Fig. 3). The nematic phase, N, formed uniform textures in thin cells treated for planar alignment, and in the N_F phase, the uniform texture was accompanied by characteristic conical defects anchored at the cell spacers.[12] In the N_{TBF} phase a striped texture was observed. The SmA_F phase produced a mostly uniform texture, with mosaic-like regions, while the textures of the SmC_F phase were heavily dependent on the preceding phase. Following the SmA_F phase, small striped domains developed from the mosaic texture, while non-characteristic and strongly scattering textures appeared on cooling from the N_{TBF} phase.

The phase assignments were supported by measurements of the temperature dependence of the optical birefringence (Fig. S1). The classification of nematic or smectic phases were confirmed by X-ray diffraction measurements. For all the phases reported here, the wide-angle X-ray diffraction signal was diffuse, confirming their liquid-like nature. The character of the low-angle diffraction signal changed from diffuse in nematic phases to sharp, with width limited only by instrumental broadening, in smectic phases, evidencing evolution of the positional order of molecules from short-range in nematics to long-range in smectics.

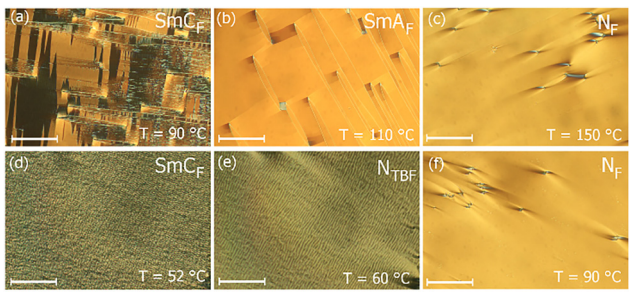

Fig. 3 Representative textures for LC phases formed by **E–1–2** (a)–(c) and **P–1–2** (d)–(f) in cells treated for planar alignment and having parallel rubbing on both surfaces. Scale bars correspond to 50 μm.

Results and discussion

The transition temperatures and phase sequences are given in Table S1 along with the values for the corresponding methoxy-substituted compounds reported previously, and the phase diagrams of the four homologous series studied are presented in Fig. 4.

All the compounds reported here formed the ferroelectric nematic phase, and all except the longer homologues of group **X–1–2** formed the paraelectric nematic phase. Mesogens which formed additional liquid crystal phases could be split into two groups, showing on cooling either a sequence of N_F–SmA_F–SmC_F or N_F–N_{TBF}–SmC_F. Measurements of the temperature dependence of the optical birefringence showed clear differences between the two phase sequences (Fig. 5). In both cases, the N–N_F phase transition was accompanied by a step-like increase in Δn due to the growth of orientational order parameter associated with the onset of polar order. For several of the materials, a pronounced dip in the optical birefringence was additionally seen at the N–N_F transition (Fig. S1), which has been previously ascribed to strong fluctuations in the orientational order at the onset of polar order.[13,14] The following transition to SmA_F phase was also accompanied by an increase in Δn due to the coupling of orientational and lamellar order (Fig. 5), while in contrast the transition to the N_{TBF} phase was associated with a decrease in Δn due to the tilting of the molecules with respect to the helical axis within the heliconical structure. The transition between orthogonal and tilted smectic phases was confirmed by change in layer spacing (Fig. 6). In the SmA_F phase, the layer spacing was essentially constant, and corresponded to the full molecular length (*ca.* 31 Å). In the SmC_F phase it continually decreased due to the tilting of molecules. In both phases, the wide-angle signal remains diffuse, indicating the lack of long-range positional correlations of molecules within the smectic planes.

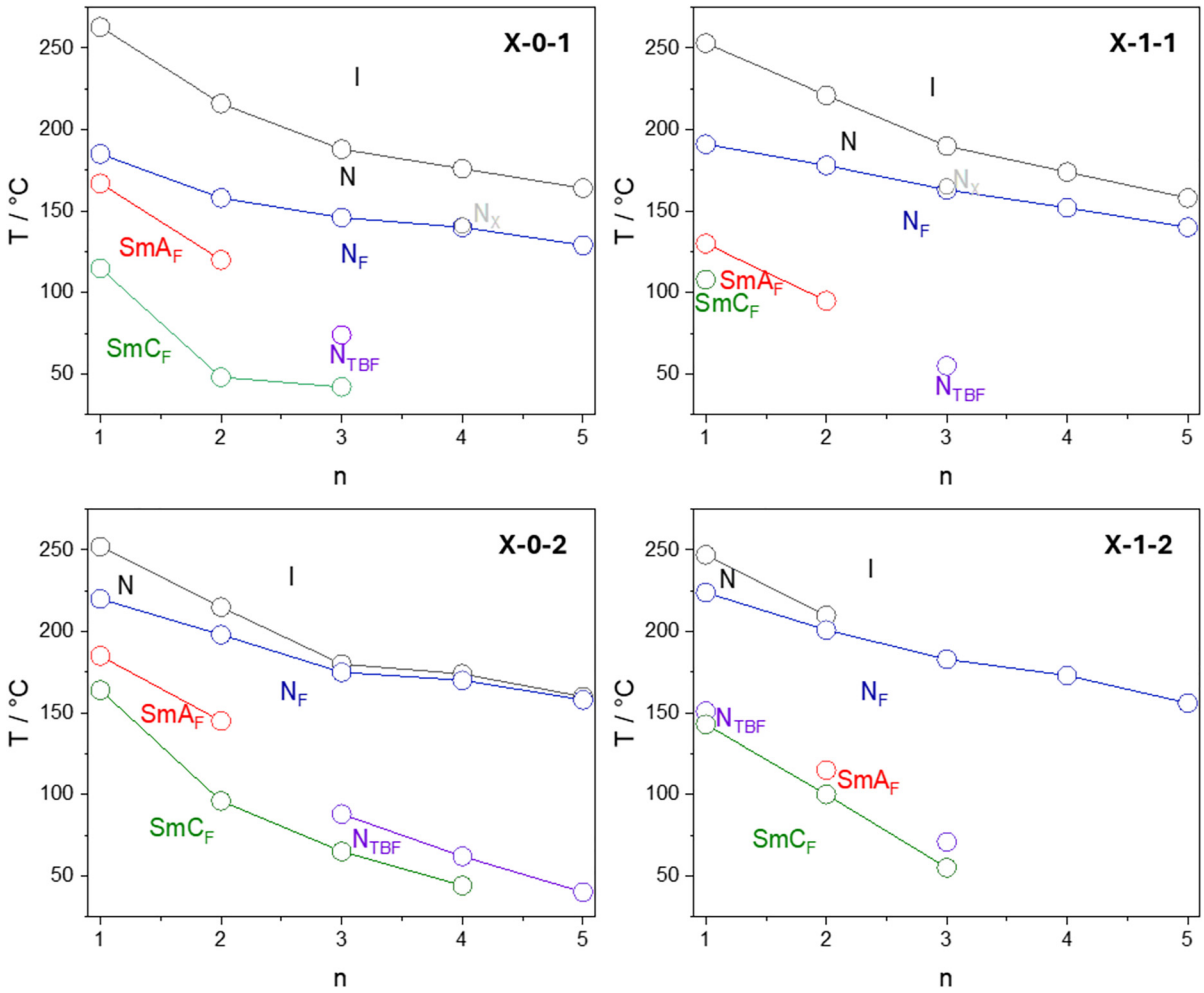

Fig. 4 The phase diagrams for the four homologue series reported here. The phase transition temperatures are presented as a function of the number of carbon atoms in the lateral chain, *n*.

The polar character of liquid crystal phases was established through dielectric spectroscopy and polarisation switching measurements. Although the precise physical interpretation of measured permittivity is highly complex for such phases, qualitative trends can clearly be seen (Fig. S2). A very strong relaxation mode is detected in the N_F phase in all studied materials, the intensity of which drops off sharply on entering the SmA_F phase, before rebuilding on transition to the SmC_F phase. In contrast, the changes at the N_F–N_{TBF} phase transition are much more subtle, with a gradual decrease seen in the strength and relaxation frequency of the mode. Unfortunately, all the materials studied crystallised before reaching the N_{TBF}–SmC_F transition when performing dielectric spectroscopy experiments. All polar phases gave clear switching current peaks associated with polarisation reversal upon application of ac electric field, and representative examples are given in Fig. 7. In the N_{TBF} and SmA_F phases there is a single current peak per half cycle of applied triangular-wave voltage, while in the SmC_F phase an additional small peak appears that is related to reduction/restoration of the tilt, this signal grows on cooling with growing tilt angle.[10,15]

The phase diagrams for the four series are shown in Fig. 4. The same trends are seen in the first three series, **X–0–1**, **X–0–2**, and **X–1–1**, the shortest, methoxy-substituted homologues of which showed the same phase sequence: N–N_F–SmA_F–SmC_F. Increasing the length of the lateral alkoxy chain led to a decrease in both T_{NI} and T_{NFN}, with the former decreasing more rapidly. These trends are in good agreement with those previously reported for ferroelectric nematic liquid crystals and are related to the decreasing molecular shape anisotropy.[16] The temperature of the N_F–SmA_F and SmA_F–SmC_F transitions also decreased strongly with replacing the methoxy chain with an ethoxy one, to such an extent that for **E–1–1** the SmC_F phase was not seen at all prior to crystallisation. Interestingly, increasing the length of the lateral chain to three carbons led to the loss of the SmA_F phase, which was replaced by the emergence of the N_{TBF} phase in all three series. For **P–0–1** and **P–0–2**, this then transitioned to the SmC_F phase on further cooling, while in **P–1–1**, the sample crystallised without forming any other LC phases.

Extending the chain length further in series **X–0–1** and **X–1–1** produced only nematic and ferroelectric nematic phases in

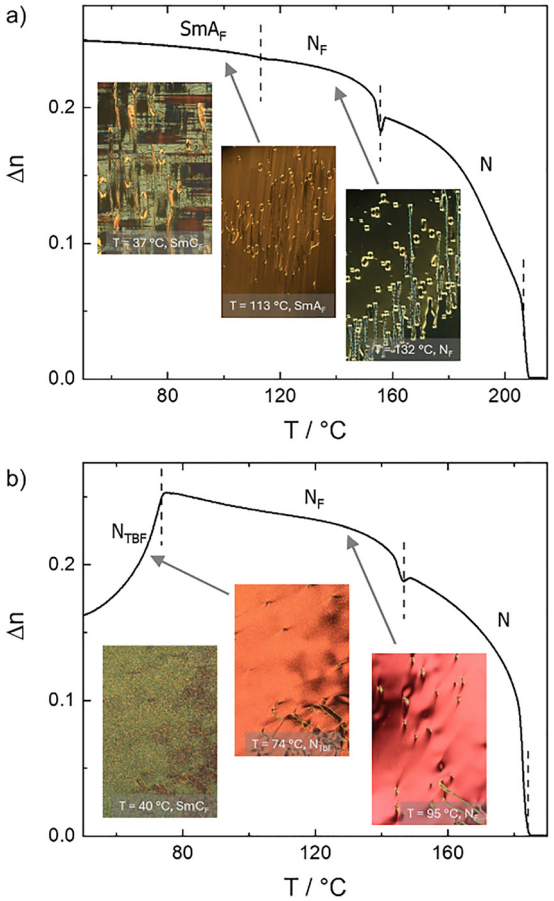

Fig. 5 The temperature dependence of the optical birefringence of: (a) **E–0–1** and (b) **P–0–1** measured with green light, note that the SmC_F phase was not reached due to sample recrystallisation during slow cooling. Inset: Example POM textures seen in cells treated for planar alignment.

the butoxy and pentoxy homologues (n = 4 and 5). This presumably reflects a further decrease in the transition temperatures to more ordered phases, such that they are not reached before the sample crystallises. In contrast, **B–0–2** forms both the N_{TBF} and SmC_F phase, and **Q–0–2** forms the N_{TBF} phase, which could be supercooled to room temperature. The transition temperatures of the ferroelectric phases formed by the **X–0–2** series are consistently higher than those of the **X–0–1** and **X–1–1** series. This highlights the sensitivity of the relationship between fluorination pattern and phase behaviour in these materials.

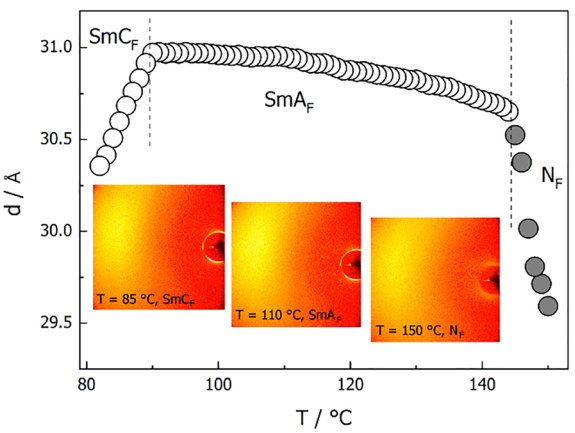

Fig. 6 The temperature dependence of the layer spacing, d, in smectic phases (open circles) and local periodicity along the director in nematic phase (filled circles), measured for **E–0–2**, with the X-ray diffraction patterns taken in the N_F, SmA_F, and SmC_F phases.

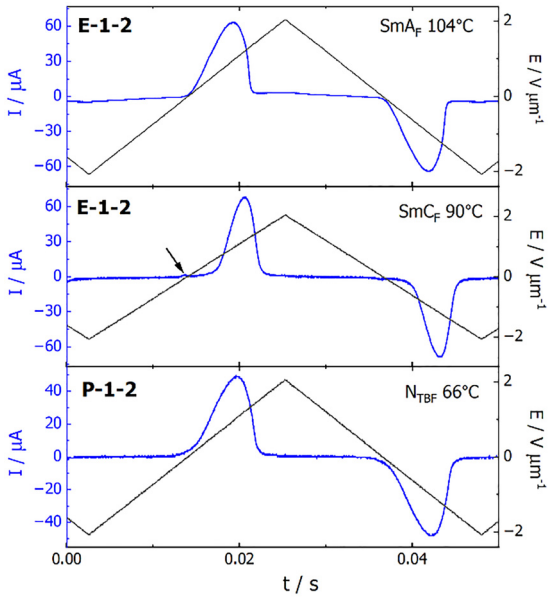

Fig. 7 Switching current recorded in the SmA_F, SmC_F and N_{TBF} phases under the application of triangular-wave voltage, observed current peaks are due to reversal of polarisation, which occurs at certain threshold field. Arrow indicates additional current peak present in the SmC_F phase, attributed to removal/restoration of molecular tilt. The magnitude of polarisation, determined by integrating the current peaks, is ~5 μC cm^{-2} in all the phases, a typical value for this class of compounds.

The phase behaviour of the final series of compounds, **X–1–2**, was more complex. The parent methoxy-substituted **M–1–2** formed the N_{TBF} phase, rather than the SmA_F phase seen in the other series. From the trends discussed above, it may be expected that increasing the length of lateral substituent would simply lead to a decrease in the N_F–N_{TBF} transition temperature, until crystallisation prevented its observation. However, the ethoxy-substituted **E–1–2** unexpectedly formed the SmA_F phase. Upon further increasing the length of the substituent to three carbons in **P–1–2**, the N_{TBF} phase reappeared and the SmA_F phase was lost. Additionally, the N phase was also not seen for this and longer homologues, with **P–1–2**, **B–1–2** and **Q–1–2** all showing direct isotropic-ferroelectric nematic transitions.

Exploring the unexpected crossover between SmA_F and N_{TBF} phases

To further investigate the apparent competition between the N_{TBF} and SmA_F phases seen in the studied materials, binary mixtures were prepared for members of the **X–1–2** series, and these are shown in Fig. 8. The first set of mixtures combined **M–1–2** and **P–1–2** (n = 1 and 3, respectively). While both pure

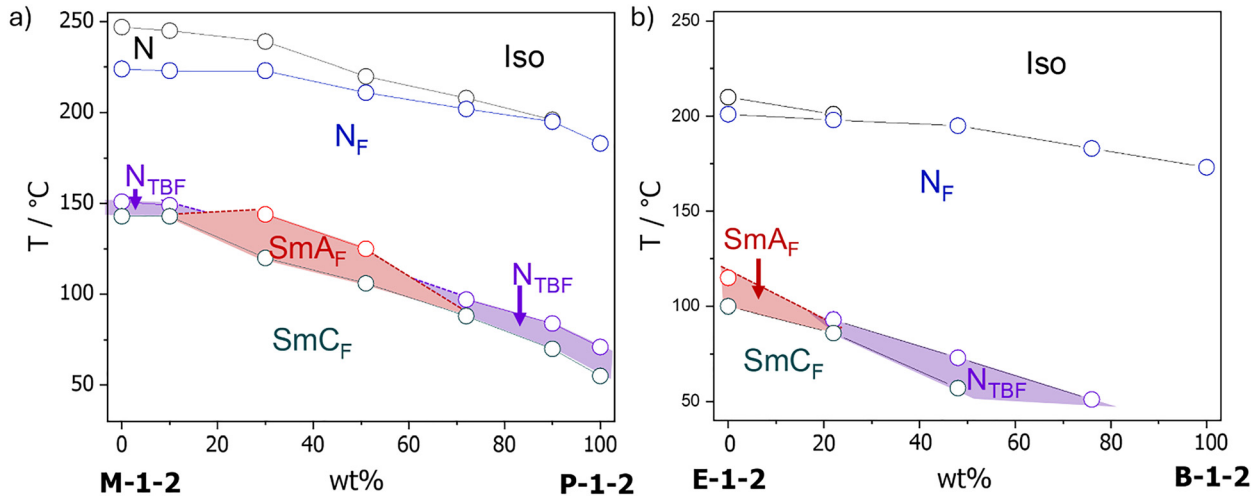

Fig. 8 Phase diagrams for binary mixtures of **M–1–2** and **P–1–2** (a) and **E–1–2** and **B–1–2** (b).

materials showed the same phase sequence N–N_F–N_{TBF}–SmC_F, in mixtures the N_{TBF} phase is replaced by the SmA_F phase, as was seen for the intermediate homologue **E–1–2** (n = 2), which can be considered as an analogue of the equimolar mixture. Similarly, mixing of **E–1–2** (n = 2, sequence N–N_F–SmA_F–SmC_F) and **B–1–2** (n = 4, only N_F phase seen) induced the N_{TBF} phase, as seen in pure **P–1–2** (n = 3). We have previously observed similar behaviour, with induction of the N_{TBF} phase in mixtures of two components not forming this phase.[10]

These observations reinforce the idea that there is a competition between the tendencies for formation of lamellar and heliconical polar structures, however the precise physical mechanisms underpinning this are not clear. We have proposed that, in this family of materials, self-segregation between fluorinated and non-fluorinated parts of the molecule drives the formation of layered polar phases.[10] For the N_{TBF} phase, it has been suggested that the spontaneous chiral symmetry breaking occurs in order to partially compensate the large molecular dipoles through the formation of heliconical structure. We have shown here that, for the series **X–0–1**, **X–1–1**, and **X–0–2**, extending the length of lateral substituents destabilises smectic layer formation, and allows for the N_{TBF} phase to emerge. A partial explanation, then, for the competition between heliconical and lamellar order may be down to their molecular structure: the large dipole moments essential for the formation of the N_{TBF} phase require a high degree of fluorination, typically concentrated on one end of the long molecular axis. However, such a concentration of fluorine substituents tends to favour formation of lamellar structure due to self-segregation of non-compatible molecular units. These two factors may contribute to the observed competition between the N_{TBF} and SmA_F phases.

Helical pitch in the N_{TBF} phase

Nearly half of the mesogens discussed here show the N_{TBF} phase. We have previously reported the methoxy-terminated **M–1–2**, for which the pitch of the helix in the N_{TBF} phase changed in a non-monotonic way with temperature. On cooling from the N_F phase it initially decreased, reaching a minimum of *ca.* 900 nm, before unwinding again on approach to the SmC_F phase. Attempts to measure the helical pitch by laser light diffraction for any of the new materials reported here proved challenging, as the helical pitch appears to be shorter and winds more quickly in these materials, going out of detection limit *ca.* 1 or 2 K below the N_F–N_{TBF} phase transition. This decrease in the helical pitch compared to **M–1–2** can be attributed to the lower transition temperatures of the N_{TBF} phase in the new compounds. To investigate this more closely, the helical structure of compound **P–0–2** was studied by measuring selective light reflection (Fig. 9). The wavelength of selective reflection (λ_{sel}) can be related to the helical pitch (p) using the relation $\lambda_{sel} = np$, where n is the average refractive

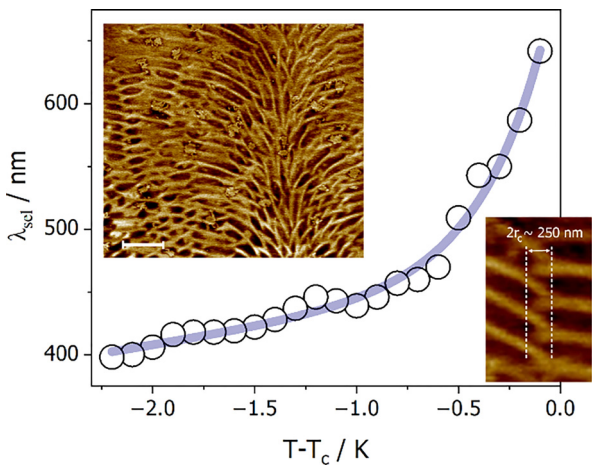

Fig. 9 The temperature dependence of the selective reflection wavelength measured in the N_{TBF} phase of **P–0–2** on cooling. Insets: 2D AFM image (height) recorded for **Q–0–2** compound at room temperature in N_{TBF} phase, the scale bar is 500 nm, the basic periodicity of pseudolayers is 250 nm and reflects helical pitch of the N_{TBF} structure. The pseudolayers are connected by screw dislocations running in the plane of the picture (inset in right bottom corner), the core size of which is comparable to the helical pitch length.

index. Assuming a value of 1.5 for n, this indicates that the pitch of the helix decreases from approximately 430 to 265 nm within a few degrees below the N_F–N_{TBF} transition.

For two mesogens, the pentyloxy-substituted **Q–0–2** and the propyloxy-substituted **P–1–1**, the N_{TBF} phase could be supercooled to room temperature, which enabled it to be studied with atomic force microscopy (AFM). AFM imaging (inset in Fig. 9 for **Q–0–2** and Fig. S3 for **P–1–1**) revealed a structural periodicity of approximately 250 nm at room temperature. This periodicity corresponds to subtle height variations on the surface, which reflect a regular stack of equivalent slabs or ''pseudo-layers'', each one approximately equal in thickness to a single helical pitch. However, in contrast to previously studied materials, where these pseudo-layers appeared largely defect-free over wide areas with only a few edge dislocations,[17] **Q–0–2** exhibits a number of nearly equally spaced, horizontally oriented screw dislocations with Burger vector magnitude $b = 1$. The width of the dislocation core, in which the pseudolayers are strongly curved, is $2r_c \sim 250$ nm.

It remains unclear whether these screw dislocations arise during the initial nucleation and growth of the pseudo-layers of the N_{TBF} phase, or whether they are an intrinsic feature of a more complex structure—for example, a twist-grain-boundary phase derived from a helical N_{TBF} phase. Apparently, for the studied system, screw dislocations that cause a continuous shift of the layers along the defect line are relatively easy to form.

Conclusions

We have reported the synthesis and liquid crystalline properties of four homologous series of mesogens with lateral alkoxy substituents. The lengths of the lateral chains were increased up to five carbon atoms to establish how this would affect the phase behaviour. For all materials, increasing the lateral chain length decreased the clearing temperature and the onset of both polar and lamellar order. For the three series **X–0–1**, **X–0–2**, and **X–1–1**, the inclusion of a three-carbon chain leads to the extinction of the SmA_F phase, which is replaced by the heliconical N_{TBF} phase. The replacement of the SmA_F phase by the N_{TBF} phase highlights the apparent competition between the driving forces contributing to the appearance of lamellar order and heliconical structure. This is reinforced by the unexpected behaviour seen in series **X–1–2**, in which the phase sequence alternates as the length of the lateral chain increases: **M–1–2** forms the N_{TBF} phase, **E–1–2** forms the SmA_F phase, and **P–1–2** again forms the N_{TBF} phase. This underscores the extremely sensitive relationships between molecular structure and the intermolecular interactions producing either lamellar or heliconical structure in these polar LC phases. For the materials studied here, the helical pitch in the N_{TBF} phase is very short, only a few hundred nm, compared to the micron-scale pitch previously reported.[1,6,10] This is attributed to the lower temperatures at which the N_{TBF} phase is observed for these new compounds. In addition, AFM images of **Q–0–2** reveal a structured network of screw dislocations, which may indicate a potential link to more complex phase structures in this family of materials.

Conflicts of interest

There are no conflicts to declare.

Data availability

The data supporting this article have been included as part of the supplementary information (SI). Supplementary information is available. See DOI: **https://doi.org/10.1039/d5mh01674f**.

Acknowledgements

This research was supported by the National Science Centre (Poland) under the grant no. 2024/53/B/ST5/03275.

References

1 J. Karcz, J. Herman, N. Rychłowicz, P. Kula, E. Górecka, J. Szydlowska, P. W. Majewski and D. Pociecha, *Science*, 2024, **384**, 1096–1099.
2 R. J. Mandle, S. J. Cowling and J. W. Goodby, *Phys. Chem. Chem. Phys.*, 2017, **19**, 11429–11435.
3 H. Nishikawa, K. Shiroshita, H. Higuchi, Y. Okumura, Y. Haseba, S. Yamamoto, K. Sago and H. Kikuchi, *Adv. Mater.*, 2017, **29**, 1702354.
4 X. Chen, E. Korblova, D. Dong, X. Wei, R. Shao, L. Radzihovsky, M. A. Glaser, J. E. Maclennan, D. Bedrov, D. M. Walba and N. A. Clark, *Proc. Natl. Acad. Sci. U. S. A.*, 2020, **117**, 14021–14031.
5 C. J. Gibb, J. Hobbs, D. I. Nikolova, T. Raistrick, S. R. Berrow, A. Mertelj, N. Osterman, N. Sebastián, H. F. Gleeson and R. J. Mandle, *Nat. Commun.*, 2024, **15**, 5845.
6 E. Gorecka, M. Majewska, L. Fekete, J. Karcz, J. Żukowska, J. Herman, P. Kula and D. Pociecha, *Mater. Horiz.*, 2025, **12**, 5352–5356.
7 P. Kumari, B. Basnet, M. O. Lavrentovich and O. D. Lavrentovich, *Science*, 2024, **383**, 1364–1368.
8 H. Nishikawa, Y. Okumura, D. Kwaria, A. Nihonyanagi and F. Araoka, *Adv. Mater.*, 2025, **37**, 2501946.
9 T. Moriya, *Phys. Rev.*, 1960, **120**, 91–98.
10 G. J. Strachan, E. Górecka, J. Hobbs and D. Pociecha, *J. Am. Chem. Soc.*, 2025, **147**, 6058–6066.
11 H. Nishikawa, D. Okada, D. Kwaria, A. Nihonyanagi, M. Kuwayama, M. Hoshino and F. Araoka, *Adv. Sci.*, 2024, **11**, 2405718.
12 P. Kumari, B. Basnet, H. Wang and O. D. Lavrentovich, *Nat. Commun.*, 2023, **14**, 748.
13 A. Barthakur, J. Karcz, P. Kula and S. Dhara, *Phys. Rev. Mater.*, 2023, **7**, 035603.
14 T. Raistrick, R. J. Mandle, Z. Zhang, P. J. Tipping and H. F. Gleeson, *Phys. Rev. E*, 2024, **110**, 044702.
15 J. Hobbs, C. J. Gibb, D. Pociecha, J. Szydłowska, E. Górecka and R. J. Mandle, *Angew. Chem., Int. Ed.*, 2025, **64**, e202416545.
16 E. Cruickshank, R. Walker, J. M. D. Storey and C. T. Imrie, *RSC Adv.*, 2022, **12**, 29482–29490.
17 A. B. Szukalska, J. Karcz, J. Herman, D. Pociecha, E. Górecka, P. Kula and J. Myśliwiec, *Adv. Mater.*, 2025, e11648.